Arch. Metall. Mater. **69** (2024), 4, 1345-1352

DOI: https://doi.org/10.24425/amm.2024.151398

HUIHUI YU[1*], QIANG HU[1], YAPAN HUANG[1], YANQI ZENG[1], JINGXUAN JIA[2], QIANG HU[1], RUI HONG[3], YOULIANG ZHANG[1]

ENHANCED MECHANICAL PROPERTIES VIA THE INCORPORATION OF Ti IN Cu ALLOYS

The influence of Ti addition on the microstructure, mechanical properties and electrical conductivity of Cu-14Fe alloy is studied. Great emphasis has been laid on the second phase, texture and mechanical properties. No new phase other than α-Fe phase could be found in Cu-14Fe-0.1Ti alloy using XRD and SEM. With 0.1Ti addition, the distribution of α-Fe phase strip is slightly heterogeneous. Cube, s and brass texture components are largely strengthened in Cu matrix with Ti addition, while copper and goss texture components are rare in Cu matrix of both alloys. In α-Fe phases, α fiber and goss texture components are highly strengthened with Ti addition. It is found that enhanced mechanical properties are achieved in Cu-14Fe-0.1Ti alloy. In detail, with Ti addition, the yield strength and ultimate tension strength increase from 538 and 561MPa to 580 and 583MPa, respectively, while maintaining a high value of elongation to failure (6.5%). A lower equivalent grain size and a higher KAM value mainly contributes to the higher yield strengthening effect in Cu-14Fe-0.1Ti alloy. The lower equivalent grain size is derived from the small size distribution range and the small size of Cu matrix in Cu-14Fe-0.1Ti alloy. The dissolution of Ti and formation of nano second phases also improve mechanical properties. However, texture hardly plays a role in the strengthening effect. 0.1Ti addition hardly reduces the electrical conductivity of Cu-14Fe alloy, maintaining a value of 33.43 %IACS. The results in this work could provide guidance in texture evolution and property evaluation in Cu-Fe alloys.

Keywords: Cu-Fe alloy; Mechanical properties; Microstructure; Phase; Texture

1. Introduction

Nowadays, Cu-Fe alloy, harboring both the characteristics of high electrical conductivity and thermal conductivity of Cu and soft magnetic properties, high rigidity of Fe [1-6], have aroused increasing interest in the field of magnetic conductive and electromagnetic shielding industry. Cu-Fe alloy is also appropriate for magnetic conductor material such as nuclear fusion devices, particle acceleration electromagnetic emitters and high-energy synchrotron radiation light source [5]. However, Cu-Fe alloy strip possesses a low yield strength, with the yield strength generally lower than 750 MPa [3,7,8], which is greatly lower than commercial high strength copper alloys such as Cu-Be [9,10], Cu-Ti [11-14] and Cu-Ni-Sn strip [15-18]. For example, the yield strength of Cu-15Ni-8Sn-0.8Nb alloy after prior cold deformation and aging treatment can reach up to 1230 MPa [17], where the good yield strength is derived from the spinodal decomposition. The low strength has become one of the key factors restricting the development and application of Cu-Fe alloys.

Deformation and heat treatment process is effective to increase the yield strength of Cu-Fe alloys. For example, the results in Cu-6.5Fe-0.3 Mg alloy [19] show that the optimal performance (i.e. ultimate tensile strength (818 MPa), electrical conductivity (61.7%IACS), and electromagnetic shielding (85-100 dB)) is obtained by hot rolling + cold rolling + heat treatment. The optimal performance is attributed to the increased density of Fe fiber resulting from the splitting of the Fe phase during hot rolling. Liu et al [20] find that better tensile strength and better conductivity in Cu-14Fe-0.1Ag composite produced by thermomechanical processing. In addition, the yield strength of Cu-Fe laminated sheets produced by the accumulative roll bonding process increases with an increase in the number of layers at both 293 K and 77 K, and the excellent temperature dependence of the tensile properties of the Cu-Fe alloy is attributed to the Cu and Fe layers and their ultrafine grains [21]. A Cu-10 wt.% Fe-0.5 wt.% Nb alloy fabricated by casting and thermomechanical treatment is annealed at 400°C for 1 h and further aged at 450°C for 8 h, to achieve high strength of 736 MPa [22]. Drawing deformation

[1] JIANGXI ACADEMY OF SCIENCES, JIANGXI KEY LABORATORY FOR ADVANCED COPPER AND TUNGSTEN MATERIALS, NANCHANG 330096, CHINA
[2] JIANGXI RARE-EARTH ACADEMY, CHINESE ACADEMY OF SCIENCES, GANZHOU 341000, CHINA
[3] CHONGQING UNIVERSITY, SCHOOL OF MATERIALS SCIENCE AND ENGINEERING, CHONGQING 400044, CHINA

* Corresponding author: hhyu91@foxmail.com

process is also effective to improve the mechanical properties of Cu-14Fe composite [23].

Alloying element addition turns out to be another effective way to improve the yield strength of Cu-Fe alloys. For example, Y. Li [24] find in Cu-10Fe alloy that when the amount of Ag addition is 3 wt.%, the tensile strength increases by 66-230 MPa. In addition, the Cu-10Fe alloy added with 2 wt.% Si could possess the yield strength enhanced from 180 MPa to 285 MPa, in which the enhancement is derived from the microstructural refinement and the formation of secondary separated phases [1]. Addition of 0.20 wt.% Zr to deformed Cu-11.5Fe composites can increase the strength by 10 % [25]. Zhang et al [22] explore the effect of Nb addition on the microstructure and properties of Cu-10Fe alloy and find that the strength higher than 700 MPa and the good fracture elongation are attributed to nanocrystals, Nb precipitates, and Fe fibers. In the above, it is found that the addition of Ag, Nb and Si elements improves the strength of the Cu-Fe alloy. However, both Nb and Ag elements are precious metals, which are expensive and increase the costs of alloy preparation. Ti has been proved to be a friendly element for strengthening copper alloys, and the Cu-Ti alloys containing approximately 1-5 wt.% Ti show good mechanical and physical properties both at room and at elevated temperatures, and superior stress relaxation behavior [12,13]. The good properties in Cu-Ti alloy are attributed to the spinodal decomposition. However, systematic investigation upon the effect of Ti addition on microstructure and mechanical properties of Cu-Fe alloy is rare. In this work, due to the duplex phases for Cu-Fe alloy, Cu matrix and α-Fe phase are independent in Cu-Fe alloy, and when enough Ti is added to Cu-Fe alloy, Ti element might dissolve into Cu matrix and precipitate during subsequent aging process just like Cu-Ti alloy. The size of second phase of Cu-Ti alloy is on the nanometer scale, and Cu-Fe alloy possess a size of α-Fe phase on the micrometer scale. This multiscale second phase size hopes to increase the strength of Cu-Fe-Ti alloy. The results do revel an enhanced mechanical property in Cu-14Fe-Ti alloy. The relevant mechanism is discussed.

2. Experiments and methods

2.1. Sample preparation and mechanical tests

The as-cast Cu-14Fe-xTi alloys (x = 0, 0.1 wt.%) were fabricated by melting pure copper (99.99%), pure iron (99.9%) and pure titanium (99.99%) using vacuum induction furnace (ZG-0.025) under Ar atmosphere. Pure Cu was purchased from Jiangxi Copper Group Co., LTD, pure Fe was from Nanchang Iron & Steel Co. LTD, and pure Ti from Baoti Group Co. LTD. The samples were cast into a plate-shape graphite mold of 45 mm thickness. The ingot was homogenized at 930°C for 5 hours, water cooled, and surface Milled. The as-homogenized billets were cut into plates of 10 mm in thickness for multi-pass rolling. Those plates were firstly rolled from 10 to 2 mm in thickness at room temperature, then rolled from 2 mm to 0.8 mm, followed by rolling to 0.48 mm in thickness, and to 0.2 mm in final thickness. It is worth noting that the annealing at 600°C for 30 minutes was respectively performed after each thickness (2, 0.8, 0.48, and 0.2 mm) was achieved. TABLE 1 shows the compositions of different rolled alloys. Tension tests along the rolling direction of the plate (denoted as RD) at room temperature were performed on a CMT5205 machine using a strain rate of 2×10^{-3} s^{-1}. The specimens for tension tests were dog-bone shaped with a gauge length of 9 mm and across-section of 5×0.2 mm. An extensometer was used to correct the strain during tension tests. At least three samples were tested for each condition.

TABLE 1

Compositions of different rolled alloys

Alloys	Fe/wt.%	Ti/wt.%	Cu/wt.%
Cu-14Fe	13.340	—	86.660
Cu-14Fe-0.1Ti	13.180	0.095	86.725

2.2. Microstructure and texture measurements

Phase identification of the alloys was performed using X-ray diffraction (XRD, Shimadzu XRD-7000). Electron backscatter diffraction (EBSD) mapping was conducted on a scanning electron microscope (SEM, EVO18) equipped with a HKL-EBSD system using a step size of 0.1 μm combined with energy dispersive X-ray spectrometry (EDS, X-Max20). The resulting inverse pole figure map, crystallographic orientation analysis, and pole figures were processed using the commercial TSL OIM or Channel 5 software.

3. Results

3.1. Microstructure and texture

Fig. 1 shows the XRD patterns of as-rolled Cu-14Fe and Cu-14Fe-0.1Ti alloy. It can be seen that only the diffraction

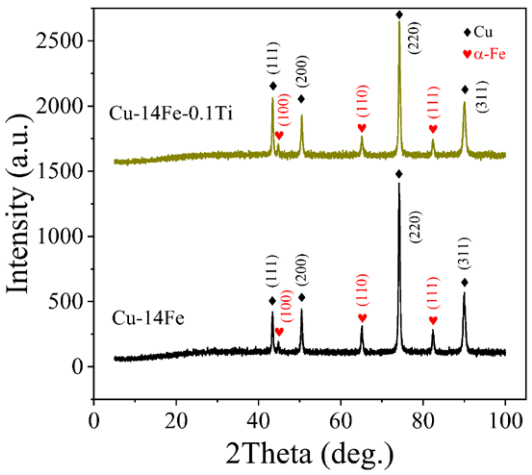

Fig. 1. XRD patterns of as-rolled Cu-14Fe and Cu-14Fe-0.1Ti alloy

peaks of the Cu matrix and α-Fe phase appear in the pattern for as-rolled Cu-14Fe and Cu-14Fe-0.1Ti alloy. Fig. 2 displays the SEM image of as-rolled Cu-14Fe and Cu-14Fe-0.1Ti alloy along the RD-ND plane, where local parts in Fig. 2a and 2b are further enlarged and provided, respectively. RD and ND denote rolling direction and normal direction of rolled plates, respectively. In Fig. 2, the dark contrast region is the Fe phase and the light contrast region is the Cu matrix. In both Fig. 2a and 2b, the α-Fe phase is distributed along the rolling direction and the large spherical Fe phase particles are deformed to a low extent. It could be seen in Fig. 2a and 2b that, the α-Fe phase strip is slightly heterogeneously distributed in Cu-14Fe-0.1Ti alloy. Combining the results from XRD patterns and EDS, no new second phase other than α-Fe phase is detected in Cu-14Fe-0.1Ti alloy using XRD and SEM.

TABLE 2

Chemical composition of phases in the rolled Cu-14Fe and Cu-14Fe-0.1Ti alloys (wt.%)

Alloy	Cu matrix			α-Fe		
	Cu	Fe	Ti	Cu	Fe	Ti
Cu-14Fe	94.15	5.85	—	13.89	86.11	—
Cu-14Fe-0.1Ti	93.95	5.38	0.67	11.50	88.27	0.23

Inverse pole figure maps and pole figures of Cu matrix and α-Fe phase in as-rolled Cu-14Fe and Cu-14Fe-0.1Ti alloy are shown in Fig. 3 and 4, with the measured texture component for Cu matrix and for α-Fe phase displayed in TABLE 3. In consistent with Fig. 2, both the Cu matrix and α-Fe phase are distributed along the rolling direction and the large spherical Fe phase particles are slightly deformed as shown in Fig. 3.

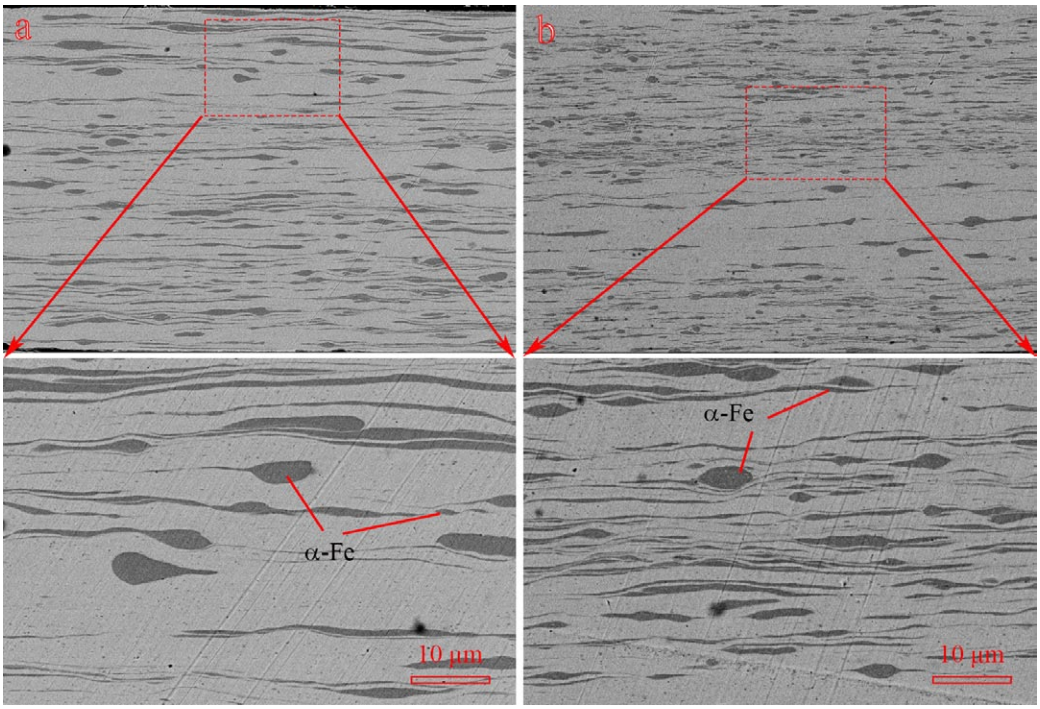

Fig. 2. SEM images of as-rolled (a) Cu-14Fe, (b) Cu-14Fe-0.1Ti alloy along the RD-ND plane, local parts in Fig. 2a and 2b are further enlarged and provided, respectively. RD: rolling direction, ND: normal direction

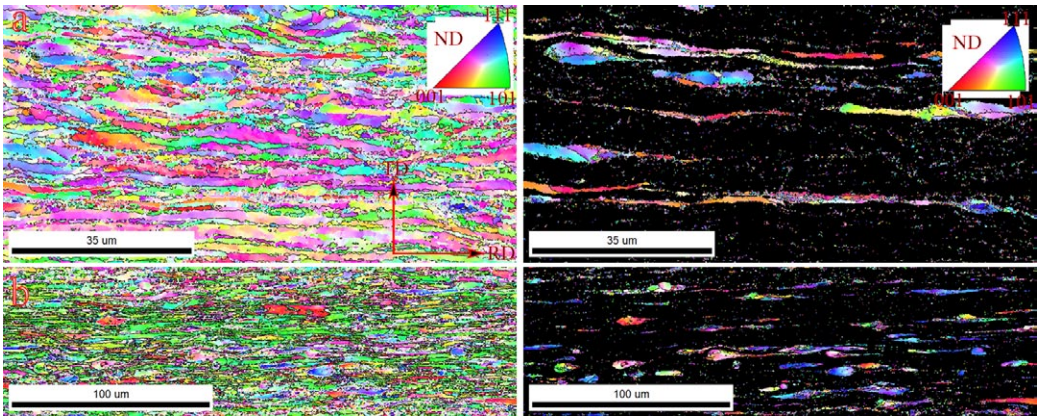

Fig. 3. Inverse pole figure maps of Cu matrix (top left corner) and α-Fe phase (top right corner) in (a) as-rolled Cu-14Fe, and of Cu matrix (lower left corner) and α-Fe phase (lower right corner) in (b) as-rolled Cu-14Fe-0.1Ti alloy. RD: rolling direction, TD: transverse direction, ND: normal direction

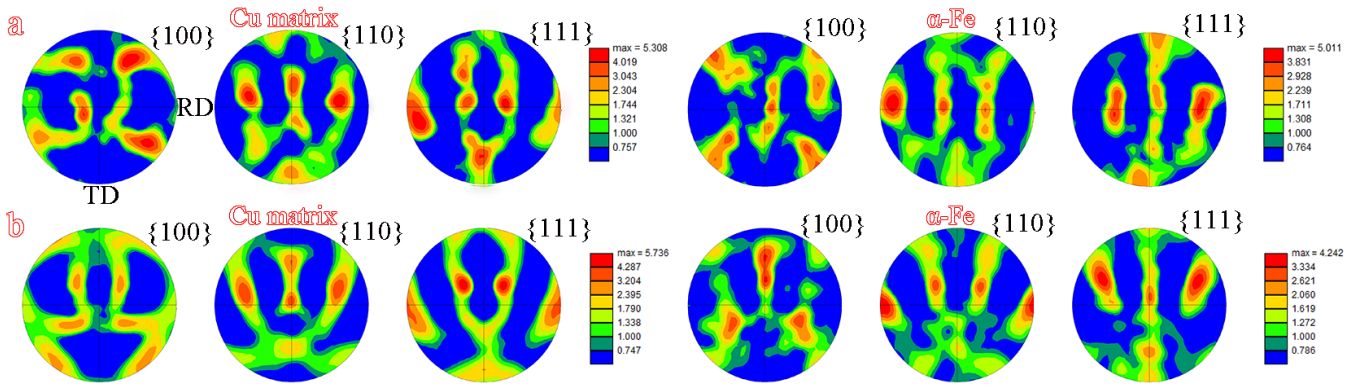

Fig. 4. Pole figures of Cu matrix and α-Fe phase in as-rolled (a) Cu-14Fe, and (b) Cu-14Fe-0.1Ti alloy. RD: rolling direction, TD: transverse direction

TABLE 3

Measured texture components and their percentages (%) in Cu matrix and in α-Fe phase

Alloy	In Cu matrix						In α-Fe phase				
	Cube	Copper	S	Brass	Goss	Rotated cube	Cube	Rotated cube	Goss	Gfiber	Afiber
Cu-14Fe	0.9	0.1	0.4	3.1	0.1	1.5	0.7	9.3	0.7	2.0	1.9
Cu-14Fe-0.1Ti	3.8	0.1	2.3	9.4	0.1	2.4	0.6	6.6	3.5	1.8	13

In addition, many fine and dispersed α-Fe phases are detected in the grain interior of Cu matrix in both alloys. Cube, s and brass texture components are largely strengthened with the addition of Ti, as shown in Fig. 4 and TABLE 3, while copper and goss texture components are rare in Cu matrix of both alloys. In α-Fe phases, α fiber and goss texture components are highly strengthened with Ti addition.

3.2. Mechanical behavior

The true stress-strain curves under tension along the rolling direction at room temperature are displayed in Fig. 5 with the relevant properties listed in TABLE 4. It is found that with Ti addition, the yield strength and ultimate tension strength increase from 538 and 561MPa to 580 and 583MPa, respectively, while Cu-14Fe-0.1Ti alloy maintains a high value of elongation to failure (6.5%). In addition, 0.1Ti addition hardly reduces the electrical conductivity of Cu-14Fe alloy, maintaining a value of 33.43%IACS (TABLE 4). It is therefore found that enhanced mechanical properties are achieved via the incorporation of Ti in Cu-14Fe alloy. It should be noted that the standard deviation of yield strength and ultimate tensile strength in Cu-14Fe-0.1Ti alloy is larger than that in Cu-14Fe alloy, implying a more heterogeneously distributed α-Fe phase in the former. This is consistent with the results shown in Fig. 2 and 3.

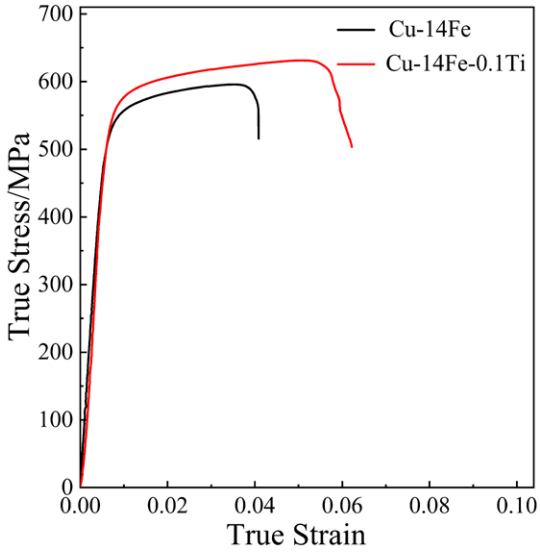

Fig. 5. True tensile stress-stain curves of as-rolled Cu-14Fe and Cu-14Fe-0.1Ti alloys under tension along the RD at room temperature

4. Discussion

Among various mechanisms responsible for the strength enhancement between duplex Cu-14Fe and duplex Cu-14Fe-0.1Ti alloy in the present work, the leading strategy is to unveil the role of α-Fe phase, those including the distribution, volume

TABLE 4

Mechanical properties under tension along the RD and electrical conductivity for different alloys

Alloy	Yield strength /MPa	Ultimate tensile strength /MPa	Elongation to failure /%	Electrical conductivity /%IACS
Cu-14Fe	538(±8.7)	561(±5.5)	4.2(±2.4)	34.07(±1.4)
Cu-14Fe-0.1Ti	580(±12.5)	583(±12.4)	6.5(±1.3)	33.43(±2.2)

fraction and size of α-Fe phase. It could be seen in Fig. 2a and 2b that, the α-Fe phase strip is slightly heterogeneously distributed in Cu-14Fe-0.1Ti alloy. According to the Energy Dispersive Spectrometer test results shown in TABLE 2, the Ti content in α-Fe phase of Cu-14Fe-0.1Ti alloy was about 0.23 wt.%, and the Ti content in the Cu matrix was about 0.67 wt.%. The composition analysis indicated that Ti was dissolved in both α-Fe phase and Cu matrix of Cu-14Fe-0.1Ti alloy, but the Ti content in the Cu matrix was higher than that in the α-Fe phase. The addition of Ti element damages the miscibility between the separated α-Fe phase and the Cu matrix, and the miscibility is associated with the distribution of second phase for immiscible alloys [4], thus explaining why the α-Fe phase is slightly heterogeneous after adding Ti. Phase distribution map and grain size distribution of as-rolled Cu-14Fe and Cu-14Fe-0.1Ti alloy are given in Fig. 6. α-Fe phase is colored in green. In this work, the area fraction is used to replace the volume fraction. The area fraction of α-Fe phase in Cu-14Fe alloy is 13.3%, in similar with that in Cu-14Fe-0.1Ti alloy as shown in TABLE 5. Since Cu-14Fe alloy has duplex phase including Cu matrix and α-Fe phase, the size and its relevant distribution of Cu matrix and α-Fe phase are also shown in Fig. 6 and TABLE 5. When grains are elongated along the rolling direction after rolling deformation, the lamella spacing is considered as the equivalent grain size. The size distribution range of Cu matrix in Cu-14Fe alloy is much larger than that in Cu-14Fe-0.1Ti alloy, implying a more homogenous size distribution of Cu matrix in Cu-14Fe-0.1Ti alloy. There is a smaller grain size about 3.16 mm of Cu matrix in Cu-14Fe-0.1Ti alloy compared with about 5.62 mm of Cu matrix in Cu-14Fe alloy. The size distribution range of α-Fe phase in Cu-14Fe-0.1Ti alloy is slightly larger than that in Cu-14Fe alloy. However, the size of α-Fe phase in both alloys is similar as seen from Fig. 6. Equivalent grain size (d_e) is used to incorporate the size of both Cu matrix and α-Fe phase using the following formula:

$$d_e = d_1 * V_1 + d_2 * V_2 \quad (1)$$

here, d_e is equivalent grain size, d_1 (d_2) and V_1 (V_2) are the size and volume/area fraction of Cu matrix and α-Fe phase, respectively. The calculated equivalent grain sizes are also shown in TABLE 5. It can be seen that the equivalent grain size of Cu-14Fe-0.1Ti alloy is 3.1 mm, smaller than that of Cu-14Fe alloy, a value as high as 5.2 mm. Grain refinement resulting from α-Fe phase should be one of the main strengthening factors in Cu-14Fe-0.1Ti alloy.

TABLE 5

Measured parameters including area fraction of α-Fe phase, equivalent grain size (d_e) and kernel average misorientation (KAM) of different alloys. KAM_{Cu} and $KAM_{α\text{-}Fe}$ denote KAM in Cu matrix and α-Fe phase, respectively

Alloy	Area fraction /%	d_e /mm	KAM_{Cu} /°	$KAM_{α\text{-}Fe}$ /°
Cu-14Fe	13.3	5.2	0.9652	0.9398
Cu-14Fe-0.1Ti	13.2	3.1	1.0669	1.0137

As shown in Fig. 4 and TABLE 3, texture components are largely changed with the addition of Ti, and it is known that texture might also be a strengthening factor, which is referred

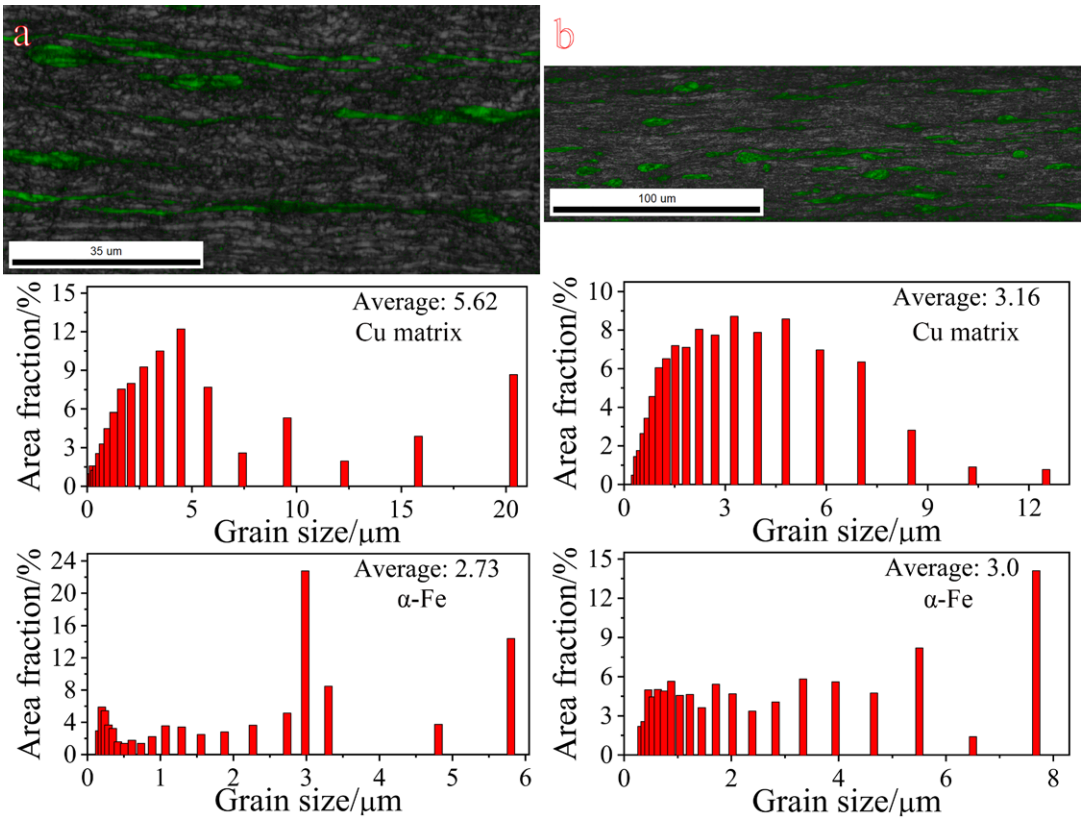

Fig. 6. Phase distribution map and grain size distribution of as-rolled (a) Cu-14Fe and (b) Cu-14Fe-0.1Ti alloy. α-Fe phase is colored in green

as the texture strengthening effect. Schmid factors (SFs) as a function of the relative spatial position in EBSD maps and relevant distribution for slip under tension along the RD for two alloys are depicted in Fig. 7, with the relevant average SF listed in TABLE 6. It is shown that for Cu-14Fe alloy, the SF is as low as 0.1818, while for Cu-14Fe-0.1Ti alloy, the SF is similar with the value to be 0.1814. The SF for α-Fe phase is also calculated as shown in TABLE 6. The SF for α-Fe phase is slightly higher than that for Cu matrix, but the value of average SF for α-Fe phase is similar for Cu-14Fe and Cu-14Fe-0.1Ti alloy. The hardness of α-Fe phase is much higher than that of Cu matrix [26], therefore, the Cu matrix would undergo plastic deformation ahead of the α-Fe phase during the yielding stage. It is therefore the SF for Cu matrix other than the SF for α-Fe phase that might play a more important role. In general, the lower the SF, the higher the texture strengthening effect. In this work, the similar SF between two alloys denotes a similar texture strengthening effect, and this implies that texture could not be an important texture strengthening effect.

Since the two alloys are in the rolled condition, stored energy in the microstructure might also lead to the yield strength increment between Cu-14Fe and Cu-14Fe-0.1Ti alloy. Usually, the Grain Average Misorientation (GAM) approach allows quantifying the dislocation density belonging to the geometrically necessary dislocations (GNDs) type and the corresponding stored energy in the microstructure [27]. KAM maps of as-rolled Cu-14Fe and Cu-14Fe-0.1Ti alloy are displayed in Fig. 8, with the value of KAM in Cu matrix and α-Fe phase shown in TABLE 5. The KAM value of Cu matrix for Cu-14Fe alloy is 0.9652°, slightly lower than that for Cu-14Fe-0.1Ti alloy, a value as high as 1.0669°. In similarity, the KAM value of α-Fe phase for Cu-14Fe alloy (0.9398°) is also slightly lower than that for Cu-14Fe-0.1Ti alloy (1.0137°). A higher KAM value in both Cu matrix and α-Fe phase indicating higher dislocation densities and a resultant higher yield strengthening effect in Cu-14Fe-0.1Ti alloy.

All in all, a low equivalent grain size and a higher KAM value mainly contributes to the higher yield strengthening effect in Cu-14Fe-0.1Ti alloy. The low equivalent grain size is derived from the small size distribution range, the small size of Cu matrix in Cu-14Fe-0.1Ti alloy and the similar size of α-Fe phase in both alloys. However, texture hardly plays a role in the

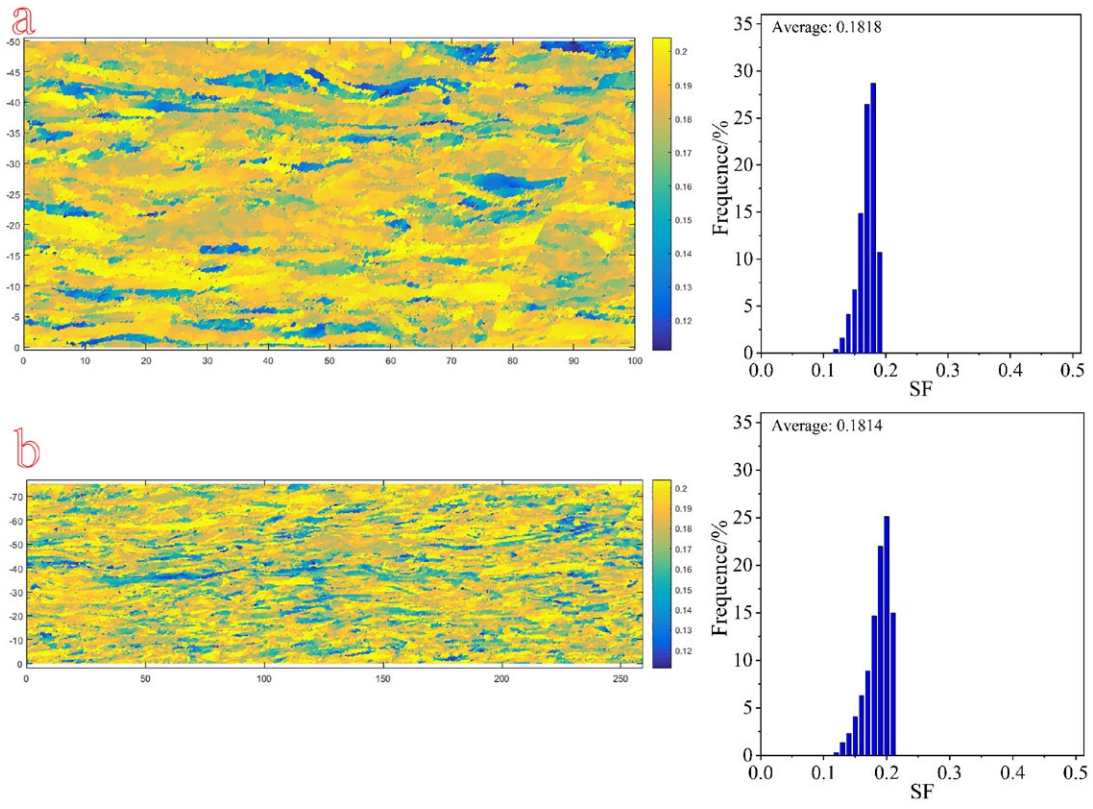

Fig. 7. Schmid factors (SFs) as a function of the spatial position in EBSD maps and corresponding distribution for slip under tension along the RD of (a) Cu-14Fe, and (b) Cu-14Fe-0.1Ti alloy

TABLE 6

The calculated average Schmid factor (SF) for Cu matrix and for α-Fe phase

Alloys	SF for Cu matrix	SF for α-Fe phase		
	{111}<1-10>	{110}<-111>	{112}<11-1>	{123}<11-1>
Cu-14Fe	0.1818	0.2518	0.2602	0.2649
Cu-14Fe-0.1Ti	0.1814	0.2573	0.2591	0.2654

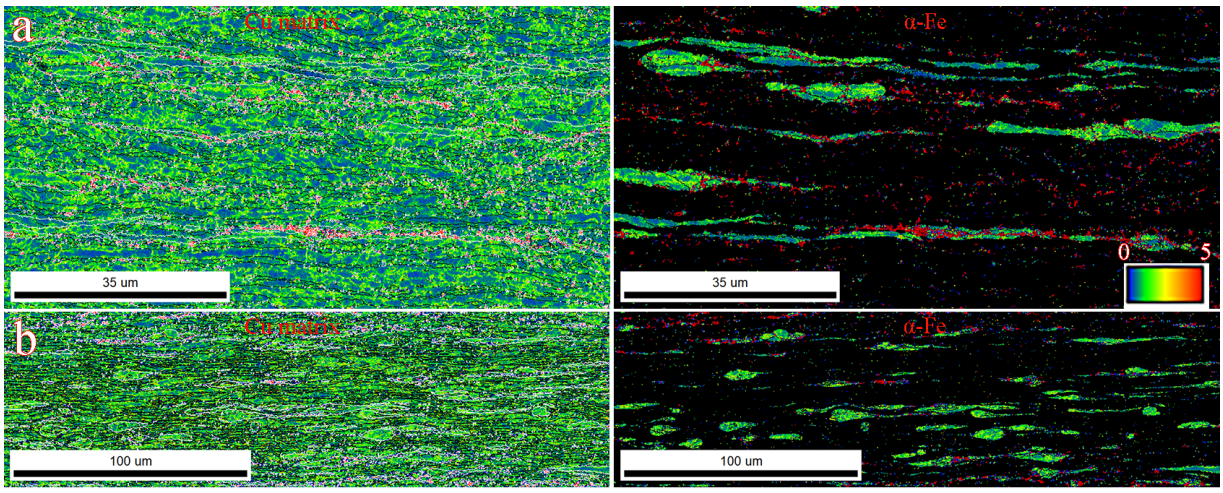

Fig. 8. Kernel Average Misorientation (KAM) maps of as-rolled (a) Cu-14Fe, and (b) Cu-14Fe-0.1Ti alloy

strengthening effect, though the texture components are highly changed in Cu-14Fe-0.1Ti alloy. In addition, it could be found from TABLE 2 that the dissolution of Ti is seen in both the Cu matrix and α-Fe phase. The dissolution of Ti in the Cu matrix and α-Fe phase change the properties of these two phases in Cu-14Fe-0.1Ti alloy, thereby might also improving mechanical properties. Besides, Ti element forms a nano second phase with Cu or Fe, while the content is too low, which is not observed in XRD and SEM, but can play a certain role in strengthening.

The electrical conductivity of Cu-14Fe alloy in the rolled state is 34.07%IACS, while the addition of 0.1Ti hardly reduces the electrical conductivity of Cu-14Fe alloy, maintaining a value of 33.43%IACS (TABLE 4). This electrical conductivity is better than Cu-Be alloy [10], Cu-Ti alloy [11], and tin-phosphor bronze. The slightly reduction in the electrical conductivity of Cu-14Fe-0.1Ti alloy is also subjected to grain refinement and higher dislocation density. In addition, the dissolution of Ti in the Cu matrix and α-Fe phase also plays a role, since it is known that the dissolution of element is more harmful to the electrical conductivity of Cu alloy in comparation with grain refinement and higher dislocation density. This also implies that the content of dissolution of Ti in the Cu matrix and α-Fe phase is low, since the electrical conductivity of Cu-14Fe-0.1Ti alloy is only slightly lower than that of Cu-14Fe alloy.

5. Conclusions

This study reports the influence of Ti addition on the microstructure evolution, mechanical properties and electrical conductivity of Cu-14Fe alloy. Great emphasis has been laid on the second phase, texture and mechanical properties. Some important conclusions have been reached:

Firstly, no new phase other than α-Fe phase could be observed in Cu-14Fe-0.1Ti alloy using XRD and SEM, in similarity with Cu-14Fe alloy. With the addition of 0.1Ti, the distribution of α-Fe phase strip is slightly heterogeneously distributed. Cube, s and brass texture components are largely strengthened in Cu matrix with the addition of Ti, while copper and goss texture components are rare in Cu matrix of both alloys. In α-Fe phases, α fiber and goss texture components are highly strengthened with Ti addition.

Secondly, it is found that enhanced mechanical properties are achieved via the incorporation of Ti in Cu-14Fe alloy. In detail, with Ti addition, the yield strength and ultimate tension strength increase from 538 and 561 MPa to 580 and 583 MPa, respectively, while Cu-14Fe-0.1Ti alloy maintains a high value of elongation to failure (6.5%). A lower equivalent grain size and a higher KAM value mainly contribute to the higher yield strengthening effect in Cu-14Fe-0.1Ti alloy. The low equivalent grain size is derived from the small size distribution range, the small size of Cu matrix in Cu-14Fe-0.1Ti alloy and the similar size of α-Fe phase in both alloys. However, texture hardly plays a role in the strengthening effect, though the texture components are highly changed with Ti addition. The dissolution of Ti along with Ti element forming a nano second phase with Cu or Fe, change the properties of these two phases in Cu-14Fe-0.1Ti alloy, thereby might also improving mechanical properties. In addition, 0.1Ti addition hardly reduces the electrical conductivity of Cu-14Fe alloy, maintaining a value of 33.43%IACS. This electrical conductivity is better than Cu-Ti alloy, Cu-Be alloys and tin-phosphor bronze.

Data availability

All relevant data supporting the findings of this study are contained in the paper and its supplementary information files. All other relevant data are available from the corresponding authors on request.

Declaration of competing interest

The authors declare that they have no known competing financial interests or personal relationships that could have appeared to influence the work reported in this paper.

Acknowledgements

This study was co-supported by the Major Scientific and Technological R&D Projects of Jiangxi Province (20212AAE01003); the Doctoral program of Jiangxi Academy of Sciences Research and Development Special Fund (2020-YYB-13); Key R & D project of Jiangxi Province (20202BBEL53022); The funding of Jiangxi Academy of Sciences (2022YSBG10001, 2022YRCS005, 2023YSBG21013); Key research and development project of Jiangxi Academy of Sciences (2020-YZD-07) and Jiangxi Academy of Sciences major Scientific research and development project (2020-YZD-2).

REFERENCES

[1] H.R. Jo, J.T. Kim, S.H. Hong, Y.S. Kim, H.J. Park, W.J. Park, M.P. Jin, K.B. Kim, J. Alloys Compd. **707**, 184-188 (2017).

[2] S. Sarkar, C. Srivastava, K. Chattopadhyay, Mater. Sci. Eng. A **723**, 38-47 (2018).

[3] H. Yu, Y. Zeng, R. Hong, Mater. Sci. **3** (1), 10-18 (2021).

[4] S. Liu, J. Jie, Z. Guo, S. Yue, T. Li, Mater. Chem. Phys. **238**, 121909 (2019).

[5] M. Wang, Y. Jiang, Z. Li, Z. Xiao, S. Gong, W. Qiu, Q. Lei, Mater. Sci. Eng. A **801**, 140379 (2021).

[6] K.X. Chen, P.A. Korzhavyi, G. Demange, H. Zapolsky, R. Patte, J. Boisse, Z.D. Wang, Acta Mater. **163**, 55-67 (2019).

[7] M. Wang, Q.-R. Yang, Y.-B. Jiang, Z. Li, Z. Xiao, S. Gong, Y.-R. Wang, C.-L. Guo, H.-G. Wei, Trans. Nonferrous Met. Soc. China **31** (10), 3039-3049 (2021).

[8] D. Yuan, H. Zeng, X. Xiao, H. Wang, B. Han, B. Liu, B. Yang, Mater. Sci. Eng. A **812**, 141064 (2021).

[9] H. Zhang, Y. Jiang, J. Xie, Y. Li, L. Yue, J. Alloys Compd. **773**, 1121-1130 (2019).

[10] R.J. Rioja, D.E. Laughlin, Acta Metall. **28** (9), 1301-1313 (1980).

[11] J.Y. Cheng, K.Z. He, M.Q. Deng, F.X. Yu, Mater. Sci. Forum **993**, 183-193 (2020).

[12] W.A. Soffa, D.E. Laughlin, Prog. Mater Sci. **49** (3-4), 347-366 (2004).

[13] S. Nagarjuna, M. Srinivas, Mater. Sci. Eng. A **406** (1-2), 186-194 (2005).

[14] S. Semboshi, T.J. Konno, J. Mater. Res. **23** (2), 473-477 (2011).

[15] B. Luo, D. Li, C. Zhao, Z. Wang, Z. Luo, W. Zhang, Mater. Sci. Eng. A **746**, 154-161 (2019).

[16] C. Zhao, W. Zhang, W. Zhi, D. Li, D. Zhang, Mater. **10** (9), (2017).

[17] O. Yi, X. Gan, L. Zhou, K. Zhou, S. Zhang, Y. Jiang, X. Zhang, Mater. Sci. Eng. A **704** (sep. 17), 128-137 (2017).

[18] Z. Guo, J. Jie, S. Liu, Y. Zhang, B. Qin, T. Wang, T. Li, Mater. Sci. Eng. A **748**, 85-94 (2019).

[19] D. Yuan, X. Xiao, X. Luo, H. Wang, B. Han, B. Liu, B. Yang, Mater. Charact. **185**, 111707 (2022).

[20] K.M. Liu, D.P. Lu, H.T. Zhou, Z.B. Chen, A. Atrens, L. Lu, Mater. Sci. Eng. A **584**, 114-120 (2013).

[21] N. Koga, S. Tomono, O. Umezawa, Mater. Sci. Eng. A **811**, 141066 (2021).

[22] P. Zhang, Q. Lei, X. Yuan, X. Sheng, D. Jiang, Y. Li, Z. Li, Mater. Today Commun. **25**, 101353 (2020).

[23] J. Zou, D.-P. Lu, Q.-F. Fu, K.-M. Liu, J. Jiang, Vacuum **167**, 54-58 (2019).

[24] Y. Li, D. Yi, J. Zhang, J. Alloys Compd. **647**, 413-418 (2015).

[25] G.E. Ji-Ping, Z.Q. Yao, S.H. Liu, Trans. Materids Heat Treat. **26** (1), 14-19 (2005).

[26] J. Moon, J.M. Park, J.W. Bae, H.-S. Do, B.-J. Lee, H.S. Kim, Acta Mater. **193**, 71-82 (2020).

[27] H. Azzeddine, T. Baudin, A.-L. Helbert, F. Brisset, Y. Huang, M. Kawasaki, D. Bradai, T.G. Langdon, J. Alloys Compd. **864**, 158142 (2021).